Hindawi
Journal of Nanomaterials
Volume 2022, Article ID 2501263, 11 pages
https://doi.org/10.1155/2022/2501263

Research Article

Impact of Homogeneous-Heterogeneous Reactions on Flow of Non-Newtonian Ferrofluid over a Stretching Sheet

H. Zeb,[1] **S. Bhatti**,[1,2] **U. Khan**,[3] **H. A. Wahab**,[3] **A. Mohamed**,[4] **and I. Khan**[3]

[1]*Department of Mathematics COMSATS University Islamabad, Abbottabad Campus, Pakistan*
[2]*University Research Center, Future University in Egypt, New Cairo 11745, Egypt*
[3]*Department of Mathematics & Statistics, Hazara University, Mansehra 21120, Pakistan*
[4]*College of Engineering Majmaah University, P.O. Box 66, Majmaah 11952, Saudi Arabia*

Correspondence should be addressed to H. A. Wahab; wahab@hu.edu.pk

Received 8 November 2021; Revised 11 July 2022; Accepted 16 August 2022; Published 2 September 2022

Academic Editor: C. L. Gan

In this study, we considered heterogeneous and homogeneous chemical reactions in Eyring-Powell ferrofluid past a stretchable surface. In addition, thermal radiation and magnetic dipole impacts are also considered. The direct numerical solution of the governing model is complex. For this, we simplified the model into coupled ordinary differential equations (ODEs) with the dimensionless variables. Then, we determined the computational solution of the resulting transformed ODE system via the Runge-Kutta (RK) method. The impacts of interesting engineering parameters on temperature, velocity, and concatenation behaviors are presented through graphs. We concluded that the velocity field is reduced for higher values of ferromagnetic parameter β and fluid material parameters β and H and arises the temperature field for higher values of thermal radiation R while the temperature field is reduced for Prandtl number Pr and dissipation parameter λ_1. The obtained results of the current work are compared with published work, and we found that between them a good agreement can be seen in the table. The characteristics of skin fraction and Nusselt number are presented.

1. Introduction

The boundary layer flows are classified into non-Newtonian and Newtonian fluid materials. The fluids in which the stress is linearly proportional to the strain are known as Newtonian fluids while those otherwise are non-Newtonian materials. Mineral oil, gasoline, water, kerosene, organic materials, glycerin, solvents, and alcohol are examples of the Newtonian fluid materials. The modeling of non-Newtonian fluid has high attention due to their high range of uses in manufacturing phenomena, geothermal engineering, and industrial processes. The nuclear reactors, spinning of fibers, metallurgical processes, casting, crystal growth, liquid metal space technology, etc. are uses of these applications. The modeling of non-Newtonian fluid phenomena cannot be captured in a single relation because of their aspects. Different models are characterized for the aspects of non-Newtonian fluids considered. The modeling of non-Newtonian fluids is classified into subclasses such as (i) differential type, (ii) rate type, and (ii) integral type. The Maxwell fluid, Carreau fluid, and Burger fluid do not clarify the properties of the rheological fluid model. So therefore the focus of our present work is an assumed Eyring-Powell fluid model [1].

The Powell-Eyring has several advantages of using at low and high shear rates and can be reduced to the Newtonian fluid by the derivation of the kinetic theory of liquids. The heat transfer modeling of an Eyring-Powell fluid has entrusting applications in thermal insulation, geophysical process and environmental pollution. Human blood, ketchup, toothpaste, etc. are the examples of Powell-Eyring fluid. Ghaffar et al. [2] studied the modeling of convection heat transfer in Eyring-Powell fluid past a vertical sheet. Najeeb et al. [3] expressed the homotopy solution for Eyring-Powell fluid flow with nanoparticles over a vertical channel. Hina et al. [4] analyzed the effects of viscose dissipation and thermophysical on Powell-Eyring fluid along the curved channels with nanoparticles. Taseer et al. [5] reported the significance

of Arrhenius activation energy on the 3-dimensional flow of an Eyring-Powell fluid with nonlinear thermal radiation. The MHD flow modeling of non-Newtonian fluid with stratified boundary was proposed by Reddy et al. [6]. The activation energy in heat and mass transfer of Eyring-Powell fluid along by taking the stretching surface is explored by Nisar et al. [7]. The modeling of convective heat and momentum slip boundary conditions in nanofluid was determined by Wang et al. [8]. The nonlinear thermoradiator heat flux in the time-dependent flow of an Eyring-Powell fluid with variable thermophysical effects was reported by Khatshwa et al. [9]. The magnetic field non-Newtonian fluid under the assumption of internal energy was proposed by Bilal et al. [10].

The ferrofluid is a nanofluid consists of ferrite nanoparticles and base fluid. Initiating the investigation of ferromagnetic fluids is developed by Stephen et al. [11] in 1965. Ferrofluid has enormous uses in industrial engineering, biological sciences, and chemical engineering. Some common uses of ferrofluid generate rotating X-ray tubes, hi-fi speakers, sensors, targeting/tumors cancer cells, accelerometer, magnetized devices, optical applications, and sensors (hard plates and recording procedures), which are used in biological processes. The combination of impacts of thermal radiation and magnetic field on viscous flow of ferrofluid was explored by Neuringer et al. [12]. The computational study of heat transfer modeling in magnetic dipole of ferrofluid past a stretchable surface was considered by Sharma et al. [13]. The heat transfer phenomena and magnetic dipole in a ferrofluid flow over a stretching surface were identified by Majeed et al. [14]. The heat transfer modeling in stratified flow of ferrofluid over a stretching sheet was demonstrated by Noor et al. [15]. Ashraf et al. [16] explored the combination of momentum slip phenomena in hybrid nanofluid by considering curved sheet. The nonlinear thermal radiating flow of ferrofluids over a moving plate with magnetic dipole effects was identified by Ali et al. [17]. The combined effects of thermodiffusion on generalized fluid with nanomaterials was analyzed by Souayeh et al. [18]. The simulation of Cattaneo and Christov heat flux modeling in ferromagnetic fluid with nanoparticles behaviors was demonstrated by Shehzad et al. [19]. The related study of ferrofluid in detail can be seen in Refs. [20–27].

Generally, homogeneous and heterogeneous reactions are concerned with natural chemical reaction processes. Some chemical reactions are very slow without a catalyst. The heterogeneous and homogeneous reactions are very complex because of their interaction in the volume of the fluid and catalyst surface, i.e., reactions produced in combustion, catalysis, and biochemical processes. The importance of chemical reactions is found in hydrometallurgical industries, mist development, food processing and diffusing, crop damaging through freezing, hardware configuration, plantation of fruit trees, and many more. Some examples of homogeneous and heterogeneous reactions are represented by Williams [28–31]. The effects of a chemical reaction and stagnation point in the boundary layer flow were presented by Chaudhary et al. [32]. Pop and Khan et al. [33] presented the viscoelastic fluid affected by homogeneous and heterogeneous reactions. Merkin et al. [34] presented that the isothermal boundary layer flow is affected by homogeneous and heterogeneous reactions. MHD flow of a second-grade fluid is affected by homogeneous and heterogeneous reactions with the porous medium reported by Cortell et al. [35]. The Newtonian heating effects on the heterogeneous and homogeneous reactive flow of non-Newtonian fluid over a stretching sheet were reported by Imad et al. [36]. Zero mass flux effects in bioconvective nanofluid over a stretching surface with response surface methodology were explored by [29]. Nanofluid flow is affected by chemical reaction and nonlinear thermal radiation over a curved surface presented by Ramzan et al. [37].

In the above literature review, we are interested to explore the heterogeneous and homogeneous reaction in non-Newtonian ferrofluid over a stretching surface. Further, the effects of thermal radiation and magnetic dipole are also determined. Here in this work, we transformed the governing model into a coupled nonlinear ODE system by similarity variables. The governing equations are computationally evaluated using shooting method with RK method.

2. Mathematical Model

We have considered heterogeneous and homogeneous reaction phenomena of Eyring-Powell ferrofluids over a stretching surface. Further, the characteristics of magnetic dipole and internal energy are assumed. The surface is to be considered along at (x, y) with velocity components (u, v); it is placed normal to the sheet in Figure 1. Here, place a magnetic dipole with the center y-axis by the displacement γ_1 from the sheet. The magnetic dipole is assumed along the positive x-axis. The magnetic field strength is arising because leading the magnetic dipole is situated to ferrofluid. Here, consider a uninformed temperature to the sheet T_w and Curie temperature T_c, whereas the fluid element is assumed in the ambient temperature $T_\infty = T_c$. So it is unable to magnetize until they initiate to cooling upon entering the sheet at the boundary layer region.

Here, we assume the interaction between the (homogeneous and heterogeneous reactions) chemical reaction with chemical reactants $\mathscr{B}$ and $\mathscr{A}$ seen in the study of boundary layer flows introduced by Merkin et al. [34]. It can be represented as follows. The homogeneous (bulk) reaction is formulated as

$$\begin{aligned} \mathscr{A} + 2\mathscr{B} &\longrightarrow 3\mathscr{B}, \quad \text{rate} = \kappa_1 a b^2, \\ \mathscr{A} &\longrightarrow \mathscr{B} \quad \text{rate} = \kappa_2 a. \end{aligned} \tag{1}$$

Here, in the above formulation, a, b are concentration of the chemical species $\mathscr{B}$ and $\mathscr{A}$, where κ_1 and κ_2 represent rate constants.

The mathematical formulation of the two-dimensional law conservation of momentum can be expressed as follows:

$$\rho \frac{d\mathbf{V}}{dt} = \nabla . \mathbf{T} + \vec{\mathscr{F}}, \tag{2}$$

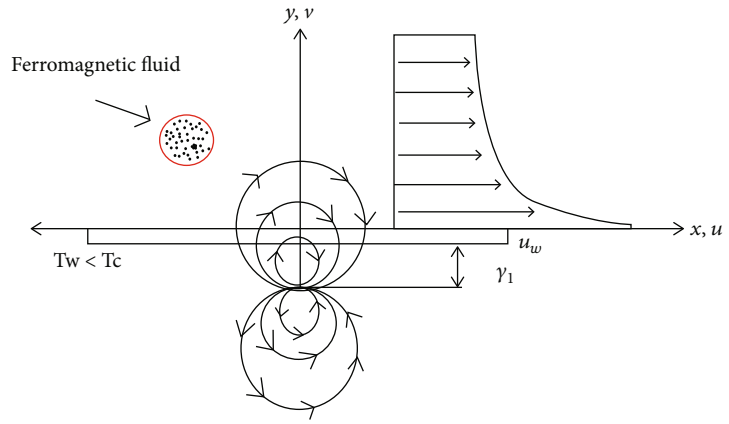

Figure 1: Geometrical configuration of the fluid problem.

where ρ, $\mathbf{V}$, and $\mathbf{T}$ represent the density, velocity, and Cauchy stress tensor. The stress tensor is stated as $\mathbf{T} = \mathbf{S} - P\mathbf{I}$, where P is taken for pressure, $\mathbf{I}$ is the identity, $\mathbf{S}$ is the extra stress tensor, and $\vec{\mathscr{F}} = \mu_o \mathscr{M} \cdot \nabla \mathscr{H}$. $\vec{\mathscr{F}}$ the body force which represents the action of magnetic field and μ_o magnetic permeability can be seen in [38]. The modeling of an Eyring-Powell fluid is formulated as follows by Siddque et al. [39] in the form

$$\mathbf{S} = \mu_o \mathbf{A}_1 + \mathbf{A}_1 \frac{1}{\dot{\gamma}\Gamma} \sinh^{-1}\left(\frac{\dot{\gamma}}{c}\right), \tag{3}$$

where Γ, μ, and c are the fluid material, viscosity, and dynamic constant, $\dot{\gamma} = \sqrt{0.5tr(\mathbf{A}_1^2)}$, $\mathbf{V} = (u(x, y, 0), v(x, y, 0), 0)$, and $\mathbf{A}_1$ is taken for a Rivlin-Ericksen tensor. It is formulated as

$$\mathbf{A}_1 = \text{grad } \mathbf{V} + \text{grad } \mathbf{V}^{T^*}. \tag{4}$$

The consideration of the rating process is to determine the formulation of an Eyring-Powell model (1994) investigated in [40–42] which also considered the shear stress of an Eyring-Powell ferrofluid model given by

$$\sinh^{-1}\left(\frac{\dot{\gamma}}{c}\right) \cong \frac{1}{c}\left(\frac{\partial u_i}{\partial u_j}\right) - \frac{1}{6c^3}\left(\frac{\partial u_i}{\partial u_j}\right)^3. \tag{5}$$

By implementing the above consideration and the boundary layer approximation leads to the governed fluid being also studied in the model [38, 43, 44]. The heat and mass transfer modeling generalized Newtonian fluid with magnetic dipole is stated as follows:

$$\frac{\partial v}{\partial y} + \frac{\partial u}{\partial x} = 0, \tag{6}$$

$$\frac{\partial u}{\partial y} v + \frac{\partial u}{\partial x} u = \frac{\mathscr{M}\mu_o}{\rho}\frac{\partial \mathscr{H}}{\partial x} + \left(\nu + \frac{1}{\rho\Gamma c}\right)\frac{\partial^2 u}{\partial^2 y} - \frac{1}{2\rho\Gamma c^3}\left(\frac{\partial u}{\partial y}\right)^2\left(\frac{\partial^2 u}{\partial y^2}\right), \tag{7}$$

$$\frac{\partial T}{\partial y} v + \frac{\partial T}{\partial x} u + T\frac{\mu_o}{\rho Cp}\frac{\partial \mathscr{M}}{\partial T}\left(u\frac{\partial \mathscr{H}}{\partial x} + v\frac{\partial \mathscr{H}}{\partial y}\right) + \frac{1}{\rho c_\rho}\frac{\partial q_r}{\partial y} = \frac{\kappa}{\rho Cp}\frac{\partial^2 T}{\partial y^2}, \tag{8}$$

$$v\frac{\partial a}{\partial y} + u\frac{\partial a}{\partial x} = \mathscr{D}_{\mathscr{A}}\frac{\partial^2 b}{\partial y^2} - K_s ab^2, \tag{9}$$

$$v\frac{\partial b}{\partial y} + u\frac{\partial b}{\partial x} = \mathscr{D}_{\mathscr{B}}\frac{\partial^2 b}{\partial y^2} + K_s ab^2. \tag{10}$$

Here, (u, v) represents the velocity components along the (x, y)-axes, while T is taken for temperature of the fluid. Further, κ, $\mathscr{D}_{\mathscr{A}}$, $\mathscr{D}_{\mathscr{B}}$, μ, and μ_o represent the thermal conductivity, diffusion species coefficients, dynamic viscosity, and magnetic permeability, respectively. The boundary conditions are given by

$$u(x, y) = u_w(x) = dx, \quad v(x, y) = 0, \quad T = T_c - T_w = \mathscr{A}\left(\frac{x}{1}\right)^2, \mathscr{D}_{\mathscr{A}}\frac{\partial a}{\partial y} = \kappa_d a, \mathscr{D}_{\mathscr{B}}\frac{\partial b}{\partial y} = -\kappa_d a, \text{ at } y = 0,$$
$$u(x, y) \longrightarrow 0, \frac{\partial u}{\partial y} \longrightarrow 0, \quad T \longrightarrow T_\infty, \quad a = a_0, b = 0, \quad \text{as} \quad y \longrightarrow \infty. \tag{11}$$

The radiation term $\tilde{q}_r$ in Equation (8) is expressed in Ref. [45] as

$$\tilde{q}_r = -\frac{4\varsigma}{3d^*}\frac{\partial T^4}{\partial y}. \tag{12}$$

Here, ς and d^* are for the Stefan Boltzmann constant absorption coefficient. We assumed the relation between the fluid temperature and the fluid temperature far away is assumed from the sheet to be a linear function. Utilizing the Taylor series expression of T^4 about T_∞, we can define

$$T^4 \approx -\left(\frac{3}{4}T_\infty - TT_\infty^3\right). \tag{13}$$

Utilizing Equation (12) in Equation (13), we obtained

$$\tilde{q}_r = \frac{4\varsigma}{3d^*}T_\infty^3\frac{\partial T}{\partial y}. \tag{14}$$

3. Magnetic Dipole

The magnetic dipole variation under the consideration of magnetic field can be settled by the function known as magnetic scalar potential explored in Refs [12, 14, 46]. It can be expressed as

$$\Phi = \frac{\gamma_2}{2\pi}\frac{x}{x^2 + (y+\gamma_1)^2}. \tag{15}$$

Here, γ_2 represents magnetic field strength; $\mathscr{H}_x$ and $\mathscr{H}$ take the magnetic field intensity at (x, y)-axis, and it is given by

$$\mathscr{H}_x = -\frac{\partial\Phi}{\partial x} = -\frac{\gamma_2}{2\pi}\frac{-(\gamma_1+y)^2 + x^2}{\left((\gamma_1+y)^2 + x^2\right)^2}, \tag{16}$$

$$\mathscr{H}_y = \frac{\partial\Phi}{\partial y} = \frac{\gamma_2}{2\pi}\frac{2x(\gamma_1+y)}{\left((\gamma_1+y)^2 + x^2\right)^2}. \tag{17}$$

Generally, this is known as the magnetic force which is gradient of a magnetic field $\mathscr{H}$. It is expressed by

$$\mathscr{H} = \sqrt{\left(\frac{\partial\Phi}{\partial x}\right)^2 + \left(\frac{\partial\Phi}{\partial y}\right)^2}. \tag{18}$$

Using Equations (15) and (17) in (18), we obtain

$$\frac{\partial\mathscr{H}}{\partial x} = -\frac{\gamma_2}{\pi}\frac{x}{(y+\gamma_1)^4}, \tag{19}$$

$$\frac{\partial\mathscr{H}}{\partial y} = \frac{\gamma_2}{\pi}\left(\frac{2x}{(y+\gamma_1)^5} - \frac{1}{(y+\gamma_1)^3}\right). \tag{20}$$

We considered that magnetization $\mathscr{M}$ is a linear function at given temperature. It is presented as

$$\mathscr{M} = -\mathscr{K}_p(T - T_c). \tag{21}$$

The geometrical and physical implementation of the ferrofluids can be seen in Figure 1.

3.1. Simplification of the Problem. By assuming the dimensionless variables as follows,

$$\varphi(\eta,\zeta) = f(\eta)\zeta\frac{\mu}{\rho}, \quad \vartheta(\eta,\zeta) = \frac{T_c - T}{T_\infty - T_o} = \vartheta_1(\eta) + \zeta^2\vartheta_2(\eta) \quad a = a_o g(\eta),\ b = a_o h(\eta), \tag{22}$$

here the dimensional coordinates are given as

$$\zeta = y\sqrt{\frac{\varrho d}{\mu}},$$
$$\eta = y\sqrt{\frac{\varrho d}{\mu}}, \tag{23}$$

where $\varphi(\zeta,\eta)$ and $\vartheta(\zeta,\eta)$ are the dimensionless stream function of the temperature and pressure. The velocity can be defined as

$$u = \frac{\partial\varphi}{\partial y} = df'(\eta), \tag{24}$$

$$v = -\frac{\partial \varphi}{\partial x} = -\sqrt{\frac{\mu d}{\varrho}} f(\eta). \tag{25}$$

By using the similarity transformation (22)–(24) and (15)–(21) in (6)–(9), it reduced to highly nonlinear ODEs such as

$$ff'' - f'^2 + (H+1)f''' - \frac{2\beta\vartheta_1}{(\alpha+\eta)^2} - H\beta f''^2 f''' = 0, \tag{26}$$

$$\begin{aligned}(1+R)\vartheta_1'' + \Pr\left(f\vartheta_1' - 2f'\vartheta_1\right) + 2f\frac{\beta\lambda_1(\vartheta_1-\epsilon)}{(\alpha+\eta)^3} \\ + 2\vartheta_2 - 4\lambda_1 f'^2 = 0,\end{aligned} \tag{27}$$

$$\begin{aligned}\vartheta_2''(1+R) - \Pr\left(f\vartheta_2' + 4f'\vartheta_2\right) + 2f\frac{\beta\lambda_1(\vartheta_2-\epsilon)}{(\alpha_2+\eta)^3} \\ - \lambda_1\beta(\vartheta_1-\epsilon)\left[\frac{2f'}{(\alpha+\eta)^3} - \frac{4f}{(\alpha+\eta)^5}\right] - 4\lambda_1 f''^2 = 0,\end{aligned} \tag{28}$$

$$\frac{1}{Sc}g'' + fg'^2 = 0, \tag{29}$$

$$\frac{\delta_1}{Sc}h'' + hg'^2 = 0. \tag{30}$$

The boundary and initial condition becomes

$$\begin{aligned}f'(\eta) = 1, \quad f(\eta) = 0, \vartheta_1(\eta) = 1 \quad \vartheta_2(\eta) = 0, \text{at} y = 0, f' \longrightarrow 0, \quad \vartheta_1 \longrightarrow 0, \\ \vartheta_2 \longrightarrow 0, g'(0) = K_s g(0), g(\infty) = 1, \delta h'(0) = K_a h(0), g(\infty) = 1, \text{at}\, y \longrightarrow \infty.\end{aligned} \tag{31}$$

Consider the diffusion coefficient $(\mathscr{D}_{\mathscr{B}}, \mathscr{D}_{\mathscr{A}})$ of reactants $\mathscr{B}$ and $\mathscr{A}$ is equal (i.e., $\delta_1 = 1$); see in Ref. [44]; therefore, this assumption can be expressed as

$$g(\eta) + h(\eta) = 1. \tag{32}$$

So Equations (29) and (30) can be seen in Ref. [36] and formulated as

$$\frac{1}{Sc}g'' - g'f + K_s g(g-1)^2 = 0, \tag{33}$$

with boundary conditions

$$g\frac{1}{K_a}(0) = g'(0), \quad g(\infty) = 1. \tag{34}$$

In the above calculation, f', ϑ_1, and g represent the velocity, temperature, and concentration, respectively. Further, β and λ_1 are represented the magnetic dipole and viscous dissipation parameters, respectively, $K_a = \kappa_1 a_o^2/d$ is taken for strength of homogeneous (surface) reaction, $\delta_1 = \mathscr{D}_{\mathscr{B}}/\mathscr{D}_{\mathscr{A}}$ is the ratio of diffusion coefficient, $K_s = (\kappa_2/\mathscr{D}_{\mathscr{A}} a_o)\sqrt{d/\nu}$ represents strength of heterogeneous reaction, $\mathrm{Sc} = \nu/\mathscr{D}_{\mathscr{B}}$ is the Schmidt number, $H = 1/\mu\Gamma c$ and $\beta = \varrho u_w/2xc^2\mu$ are fluid parameters, and $\Pr = \mu C_p/k_\infty$ is the Prandtl number. Further, $\lambda_1 = d\mu^2/\varrho k(T_w - T_\infty)$ is the viscous dissipation parameter, $\epsilon = T_c/(T_c - T_w)$ is the Curie temperature, $\beta = \gamma_1 \varrho \mu_o (k(T_c - T_w)/2\pi\mu^2)$ is the ferromagnetic parameter, and $\alpha = \gamma_1\sqrt{\rho d/\mu}$ is the curvature parameter.

The skin fraction coefficient C_f and local Nusselt number Nu_x are given below:

$$\begin{cases} C_f = \dfrac{\tau_w}{\varrho(u_w)^2}, \\ \mathrm{Nu}_x = \dfrac{x\tilde{q}_w}{\kappa(T_w - T_\infty)}. \end{cases} \tag{35}$$

Here, q_w and τ_w are the heat flux and skin friction, which are given as follows:

$$\begin{cases} \tau_w = \mu\left[\left(1 + \dfrac{1}{\Gamma c}\right)\dfrac{\partial u}{\partial y} + \dfrac{1}{\Gamma c^6}\left(\dfrac{\partial u}{\partial y}\right)^3\right]_{y=0}, \\ \tilde{q}_w = \left[-\kappa\dfrac{\partial T}{\partial y} - \dfrac{\partial \tilde{q}_r}{\partial y}\right]_{y=0}. \end{cases} \tag{36}$$

Here, $\tilde{q}_m$ and u_w are defined for heat transfer and for wall shear stress. The quantities stated as in Equation (20) are simplified as follows:

$$\begin{cases} C_f\sqrt{\mathrm{Re}_x} = (1+H)f''(0) - \dfrac{H\beta}{3}\left(f''(0)\right)^3, \\ \dfrac{\mathrm{Nu}_x}{\sqrt{\mathrm{Re}_x}} = -[1+R]\left(\vartheta_1'(0) + \zeta^2\vartheta_2'(0)\right). \end{cases} \tag{37}$$

3.2. Shooting Method for Our Numerical Approximation. It is a numerical scheme, which is implemented for the approximation of the boundary value problem (BVP). In the beginning, we reduce the BVP to a system of first-order initial value problems. Further, detail can be seen in Ref. [47]. The system (26) is the system of coupled ODEs of order

three in $f(\xi)$, order two in $\vartheta_1(\xi)$, order two in $\vartheta_2(\xi)$, and order two in g, respectively. The rearrangement of Equation (26) with boundary conditions in (31) will be expressed in the form

$$
\begin{aligned}
f''' &= -\frac{ff'' - f'^2 - \left(2\beta\vartheta_1/(\alpha+\eta)^2\right)}{(H+1) - \beta H f''^2},\\
\vartheta_1'' &= -\frac{\Pr\left(\vartheta_1' f - 2\vartheta_1' f'\right) + 2f\left(\beta\lambda_1(\vartheta_1 - \epsilon)/(\alpha+\eta)^3\right) + 4\lambda_1 f'^2}{(1+R)},\\
\vartheta_2'' &= -\frac{\Pr\left(\vartheta_2' f - 4\vartheta_2' f'\right) + f\left(2\beta\lambda_1(\vartheta_2 - \epsilon)/(\alpha_2+\eta)^3\right) + \lambda_1\beta(\vartheta_1 - \epsilon)\left[\left(2f'/(\alpha+\eta)^3\right) - \left(4f/(\alpha+\eta)^5\right)\right] + 4\lambda_1 f''^2}{(1+R)},\\
g'' &= Sc\left(fg' - K_s g(1-g)^2\right).
\end{aligned}
\tag{38}
$$

Now, we transform the above couple of ODEs into a first-order ODE system. So for this, we define new variables as follows:

$$
\begin{aligned}
&f = u_1, f' = u_2, f'' = u_3, f''' = u_3', \vartheta_1 = u_4, \quad \vartheta_1' = u_5, \vartheta_1'' = u_5',\\
&\vartheta_2 = u_6, \quad \vartheta_2' = u_7, \vartheta_2'' = u_7', g = u(8), g' = u(9), g'' = u'(9).
\end{aligned}
\tag{39}
$$

Using these substitutions to determine the first-order ODE system as given by

$$
\begin{aligned}
u_1' &= u_2,\\
u_2' &= u_3,\\
u_3' &= -\frac{u_1 u_3 - u_2^2 - \left(2\beta u_4/(\alpha+\eta)^2\right)}{(H+1) - \beta H u_3^2},\\
u_4' &= u_5,\\
u_5' &= -\frac{\Pr(u_1 u_5 - 2u_2 u_5) + 2u_1\left(\beta\lambda_1(u_4 - \epsilon)/(\alpha+\eta)^3\right) + 4\lambda_1 u_2^2}{(1+R)},\\
u_6' &= u_7,\\
u_7' &= -\frac{\Pr(u_1 u_7 - 4u_2 u_7) + 2u_1\left(\beta\lambda_1(u_6 - \epsilon)/(\alpha_2+\eta)^3\right) + \lambda_1\beta(\mathrm{u}_4 - \epsilon)\left(\left(2u_2/(\alpha+\eta)^3\right) - \left(4u_1/(\alpha+\eta)^5\right)\right) + 4\lambda_1 u_3^2}{(1+R)},\\
u_8' &= u_9,\\
u_9' &= \mathrm{Sc}\left(u_1 u_9 - K_s u_9(1-u_9)^2\right),
\end{aligned}
\tag{40}
$$

the boundary conditions are stated as

$$u_1 = 0, \quad u_2 = 1, u_3 = S_1, u_4 = 1u_5 = S_2u_6 = 0,$$
$$u_7 = S_3, u_8 = S_4, u_9 = K_s u_8, \text{at } \eta \longrightarrow 0 \tag{41}$$
$$u_2 = 0, u_4 = 0, u_6 = 0, \quad u_8 = 0, \text{at } \eta \longrightarrow \infty.$$

Identify the solution of these nine first-order ODE system given in Equation (41) with boundary conditions. For this, we use shooting technique with RK method; for this, we need nine initial guesses required whereas five of them are given and the other five initial guesses $u_2(\eta)$, $u_4(\eta)$, $u_6(\eta)$, $u_8(\eta)$, and $u_9(\eta)$ are defined as $\eta \longrightarrow \infty$. Hence, it is considered that $(u_3(0), u_5(0), u_7(0), u_8(0), u_9(0)) = (q_1, q_2, q_3, q_3, q_5)$. These unknown six initial guesses $(q_1, q_2, q_3, q_3, q_5)$ are simulated by iterative scheme called the Newton Rhaphson technique. The main step of this technique is we choose the suitable finite values for boundary conditions. For the convergence criteria, we are taking the step size $h = 0.02$ and tolerance TOL $= 10^{-5}$.

3.3. Validation of the Numerical Solution. In this work, we compared the results with previously published data and found good agreement between them. The comparison of skin fraction coefficient $(C_f\sqrt{\text{Re}_x})$ and Nusselt number (Nu_x) is shown in Tables 1 and 2, respectively. For this, we computed the different values of H and Pr.

4. Results and Discussions

In this work, Equations (17)–(19) are solved through shooting technique. The velocity, temperature, and concentration are analyzed and simulated in Figures 2–10. Further, the computational results of skin fraction and heat and mass transfer rate are shown in Table 3.

The importance of ferromagnetic interaction parameter β on velocity $f'(\eta)$ is shown in Figure 2. It is found that there is reduction in the velocity profile for the improved values of β. It is a fact that generally the ferromagnetic fluid is the motion of the fluid with tiny-sized firrite particles arising the viscosity of the fluid. So, the velocity of the fluid reduces for larger values of β.

Figure 3 is plotted for the characteristics of material fluid parameter H on velocity field. It is noticed that there are increases in the velocity field for H, which means the velocity and momentum boundary layer thickness. Figure 5 illustrates the velocity gradient for higher values $ß$. It is highlighted boosting the velocity field for $ß$. It is due to the direct relation between velocity of the sheet and the fluid parameter $ß$; thus, the velocity of the fluid as also increased.

Figure 4 presents the characteristics of β on temperature distribution. Here, the temperature distribution is increased for higher values of β. It is due to the interaction between the action of the ferromagnetic field and the motion of the fluids. This interaction reduces the velocity field thereby arising the frictional heating in the boundary layers. Therefore, thickness of the thermal boundary is increased.

Table 1: Comparison of $C_f\sqrt{\text{Re}_x}$ at $\beta = 0.0$, $\beta == 0$, and $H = 0.2$ with published work.

	H	Javed et al. [48]	Waqas et al. [49]	Current study
0.0	0.2	-1.0954	-1.0954	-1.09540
0.1	0.2	-1.0940	-1.0940	-1.0940
0.2	0.2	-1.0924	-1.0925	-1.09252
0.3	0.2	-1.0909	-1.0909	-1.09094
0.4	0.2	-1.0894	-1.0894	-1.08904

Table 2: Comparison of Nu_x at $H = 0.0$ and $R = \beta == 0$ for Pr with published work.

Pr	Chen et al. [50]	Iskak et al. [51]	Current study
0.72	-1.08862	-1.0885	-1.0886
1.0	-1.33330	-1.3333	-1.3333
3.0	-2.50972	-2.5097	-2.5095
10.0	-4.7968	-4.79682	-4.7943

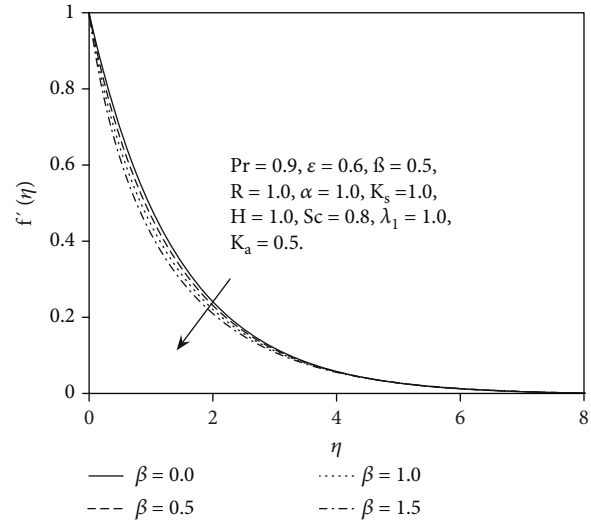

Figure 2: The properties of β on velocity field f'.

Figure 6 represents the characteristics of the temperature field for higher values (Prandtl number (Pr)). It is concluded that it declined the temperature profile for Pr. This reason is due to the fact that fluid having a small number of Pr has a high thermal diffusivity. Figure 7 shows the variation of temperature field is decreased for radiation parameter R. It is increased in temperature profile for larger values of R. This increasing occurs because of the higher temperature $\bar{T}_\infty^3$.

The outcome of frictional heating due to magnetic dipole and viscosity on the distribution of temperature imported by dissipation parameter λ_1 is shown in Figure 8. It noticed the properties of λ_1 on the temperature field. The result represents that the temperature distribution is reduced for λ_1. The reason behind that is the extraordinary behavior of ferrofluid. However, this is contrary to the case of hydrodynamic $(\beta = 0)$ although shown here that there is a rise in

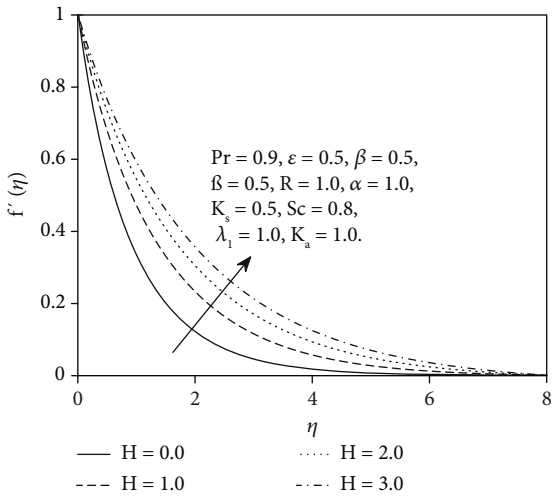

Figure 3: The velocity $f'(\eta)$ for H.

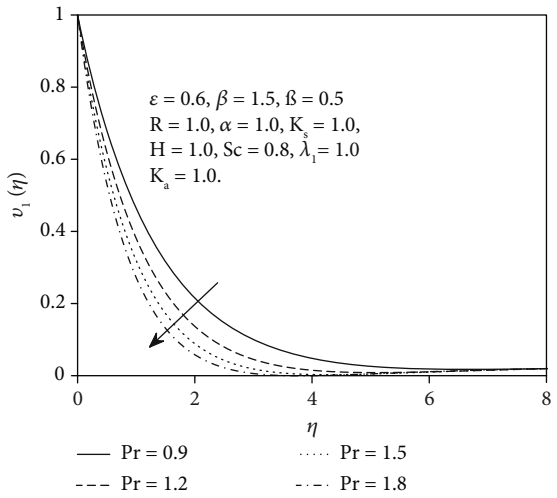

Figure 6: The variation of $\vartheta_1(\eta)$ for Pr.

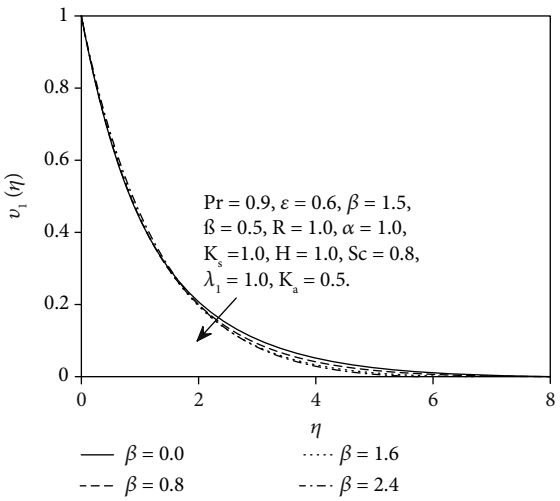

Figure 4: The characteristics of $\vartheta_1(\eta)$ for β.

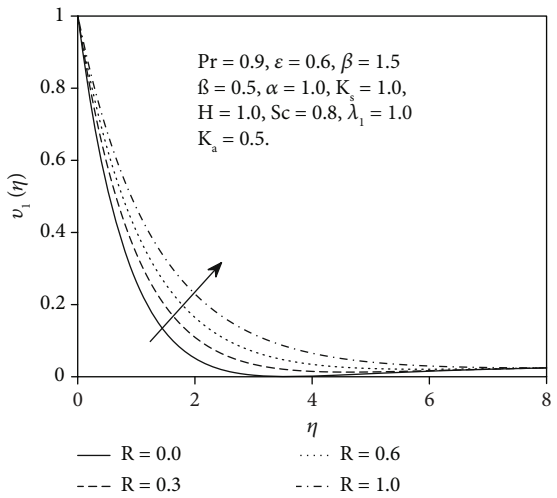

Figure 7: The impact of R for $\vartheta_1(\eta)$.

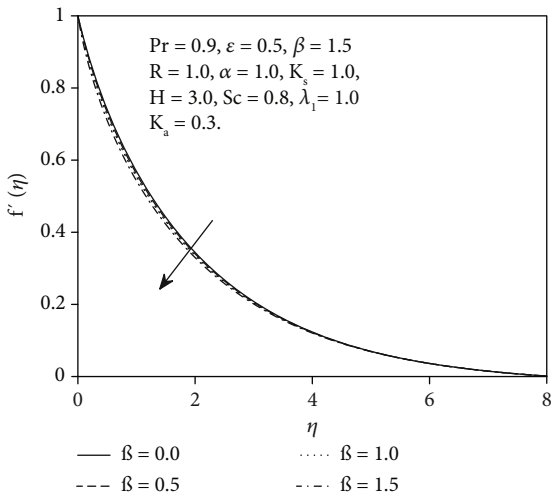

Figure 5: The characteristics of velocity field β.

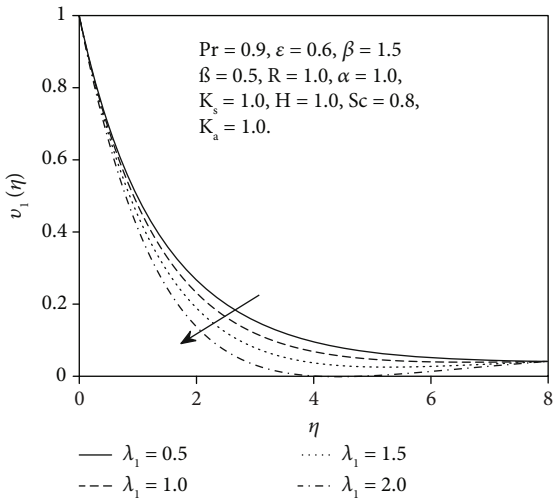

Figure 8: The impacts of $\vartheta_1(\eta)$ for λ_1.

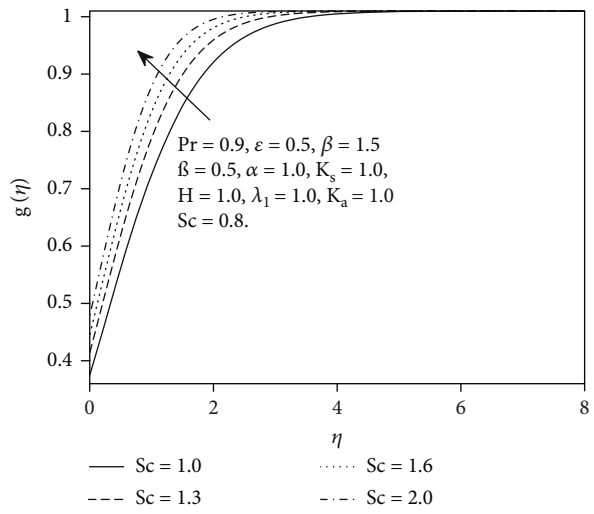

Figure 9: The impacts of Sc on g.

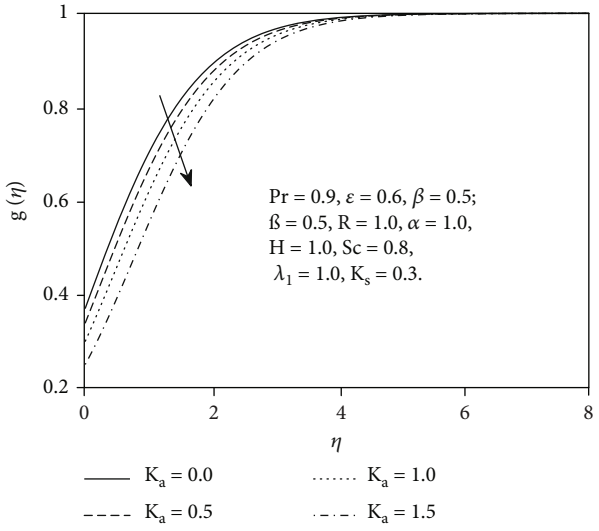

Figure 10: The impact of K_a for the distribution of temperature gradient g.

temperature distribution near the boundary layer region by enlarging the values ofλ_1. Figure 9 is designated for variation concentration gradient for the higher values of Sc. The result shows that the concentration field decreases as the Schmidt number Sc increases. Here, this impact is decreased in nanoparticle volume fraction boundary layer thickness due to the higher values of Schmidt number.

Figures 10 and 11 are made to highlight the characteristics of homogeneous and heterogeneous reactions parameters K_a and K_s on concentration behavior. It is highlighted that reduces occur in the concatenation field. It is seen that the thickness of the concentration boundary layer arises with arising the values K_s. Figure 11 is illustrated for concentration field reduced by the improving value of heterogeneous reaction K_a.

Table 3: The characteristics of skin fraction and Nusselt number for different values of Pr, β, R, λ_1, $ß$, H, and α.

Pr	β	R	λ_1	$ß$	H	α	$-f''(0)$	$\vartheta_1(0)$
4	0.2	0.3	0.1	0.4	0.6	1.6	0.59367	2.7035
1							0.52399	1.0929
2							0.52060	1.5626
3							0.51843	1.9250
	0.0						0.49007	2.2354
	0.2						0.49897	2.2341
	0.4						0.50789	2.2328
		0.0					0.49770	3.1305
		0.3					0.49822	2.7289
		0.6					0.49897	2.2341
			0.1				0.49822	2.7289
			0.3				0.49822	2.7291
			0.5				0.49822	2.7294
				0.0			0.49561	2.7296
				1.0			0.52754	2.7232
				2.0			0.59038	2.7132
					0.0		1.33322	2.5144
					2.0		0.79242	2.6546
					4.0		0.60380	2.7022
						1.0	0.60380	2.7022
						1.3	0.59623	2.7032
						1.6	0.59367	2.7035

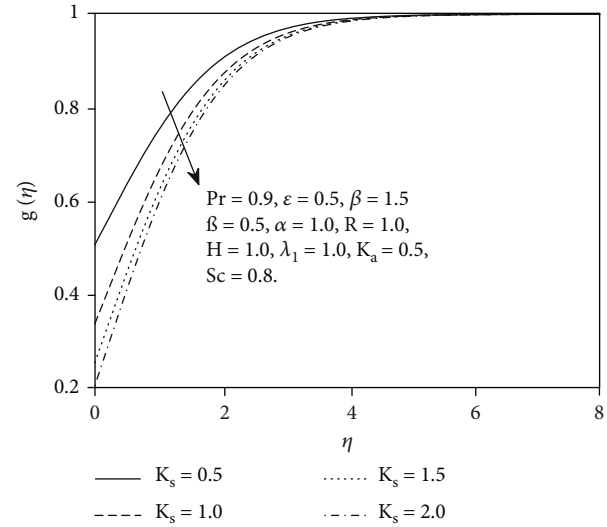

Figure 11: The properties of K_s on g.

Table 3 is made for the numerical properties of Nusselt numbers Nu_x and skin fractions C_f for different physical parameters. The skin friction increases for higher values H and λ_1 while skin friction is reduced for $ß$ and β. The Nusselt number Nu_x is increased for H, R, α, and $ß$ while it is declined for Pr and λ_1.

5. Conclusions

In this work, we analyzed heterogeneous and homogeneous reactions in Eyring-Powell ferrofluid in the existence of magnetic dipole. Further, the impacts of thermal radiation and activation energy are analyzed. The governing fluid model is transformed into higher-order ODEs by using similarity variables. The characteristics of concentration, temperature, and velocity field for interesting engineering parameters are analyzed. The heat transfer rate and skin friction coefficients are presented. The main results of the current work are listed below.

The n velocity field $f'(0)$ reduces by higher values of β and H.

There are increases in temperature field $\vartheta_1(\eta)$ for R and H while the temperature field $\vartheta_1(\eta)$ declines for the improved values of Pr.

There are increases in the concentration field $g(\eta)$ for Sc.

Conflicts of Interest

The authors declare that they have no conflicts of interest.

References

[1] H. Eyring and R. E. Powell, "Mechanisms for the relaxation theory of viscosity," *Nature*, vol. 154, no. 3909, pp. 427-428, 1944.

[2] S. Abdul Gaffar, V. Ramachandra Prasad, and B. Vijaya, "Computational study of non-Newtonian Eyring–Powell fluid from a vertical porous plate with biot number effects," *Journal of the Brazilian Society of Mechanical Sciences and Engineering*, vol. 39, no. 7, pp. 2747–2765, 2017.

[3] N. A. Khan, F. Sultan, and Q. Rubbab, "Optimal solution of nonlinear heat and mass transfer in a two-layer flow with nano-Eyring-Powell fluid," *Results in Physics*, vol. 5, pp. 199–205, 2015.

[4] S. Hina, M. Mustafa, T. Hayat, and A. Alsaedi, "Peristaltic transport of Powell-Eyring fluid in a curved channel with heat/mass transfer and wall properties," *International Journal of Heat and Mass Transfer*, vol. 101, pp. 156–165, 2016.

[5] T. Muhammad, H. Waqas, S. A. Khan, R. Ellahi, and S. M. Sait, "Significance of nonlinear thermal radiation in 3d Eyring–Powell nanofluid flow with Arrhenius activation energy," *Journal of Thermal Analysis and Calorimetry*, vol. 143, no. 2, pp. 929–944, 2021.

[6] M. Gnaneswara Reddy, M. V. V. N. L. Sudha Rani, M. M. Praveen, and K. G. Kumar, "Comparative study of different non-Newtonian fluid over an elaborated sheet in the view of dual stratified flow and ohmic heat," *Chemical Physics Letters*, vol. 784, article 139096, 2021.

[7] Z. Nisar, T. Hayat, A. Alsaedi, and B. Ahmad, "Significance of activation energy in radiative peristaltic transport of Eyring-Powell nanofluid," *International Communications in Heat and Mass Transfer*, vol. 116, article 104655, 2020.

[8] F. Wang, S. Ahmad, Q. Al Mdallal, M. Alammari, M. N. Khan, and A. Rehman, "Natural bio-convective flow of Maxwell nanofluid over an exponentially stretching surface with slip effect and convective boundary condition," *Scientific Reports*, vol. 12, no. 1, pp. 1–14, 2022.

[9] M. P. Mkhatshwa, S. S. Motsa, and P. Sibanda, "MHD mixed convective radiative flow of Eyring-Powell fluid over an oscillatory stretching sheet using bivariate spectral method on overlapping grids," *Heat Transfer*, vol. 50, no. 1, pp. 655–687, 2021.

[10] M. Bilal and M. Nazeer, "Numerical analysis for the non-Newtonian flow over stratified stretching/shrinking inclined sheet with the aligned magnetic field and nonlinear convection," *Archive of Applied Mechanics*, vol. 91, no. 3, pp. 949–964, 2021.

[11] P. S. Stephen, "Low viscosity magnetic fluid obtained by the colloidal suspension of magnetic particles," November 2 1965. US Patent 3,215,572.

[12] J. L. Neuringer, "Some viscous flows of a saturated ferro-fluid under the combined influence of thermal and magnetic field gradients," *International Journal of Non-Linear Mechanics*, vol. 1, no. 2, pp. 123–137, 1966.

[13] D. Sharma and R. C. Sharma, "Effect of dust particles on thermal convection in ferromagnetic fluid saturating a porous medium," *Journal of Magnetism and Magnetic Materials*, vol. 288, pp. 183–195, 2005.

[14] A. Majeed, A. Zeeshan, and R. Ellahi, "Unsteady ferromagnetic liquid flow and heat transfer analysis over a stretching sheet with the effect of dipole and prescribed heat flux," *Journal of Molecular Liquids*, vol. 223, pp. 528–533, 2016.

[15] N. Muhammad, S. Nadeem, and R. U. Haq, "Heat transport phenomenon in the ferromagnetic fluid over a stretching sheet with thermal stratification," *Results in physics*, vol. 7, pp. 854–861, 2017.

[16] A. Ashraf, Z. Zhang, T. Saeed, H. Zeb, and T. Munir, "Convective heat transfer analysis for aluminum oxide (Al_2O_3)- and ferro (Fe_3O_4)-based nano-fluid over a curved stretching sheet," *Nanomaterials*, vol. 12, no. 7, p. 1152, 2022.

[17] M. Ijaz, S. Nadeem, M. Ayub, and S. Mansoor, "Simulation of magnetic dipole on gyrotactic ferromagnetic fluid flow with nonlinear thermal radiation," *Journal of Thermal Analysis and Calorimetry*, vol. 143, no. 3, pp. 2053–2067, 2020.

[18] B. Souayeh, M. G. Reddy, P. Sreenivasulu, T. M. Poornima, M. Rahimi-Gorji, and I. M. Alarifi, "Comparative analysis on non-linear radiative heat transfer on MHD Casson nanofluid past a thin needle," *Journal of Molecular Liquids*, vol. 284, pp. 163–174, 2019.

[19] S. A. Shehzad and M. Gnaneswara Reddy, "Behavior of ferromagnetic Fe_2SO_4 and titanium alloy Ti_6Al_4v nanoparticles in micropolar fluid flow," *International Communications in Heat and Mass Transfer*, vol. 117, article 104769, 2020.

[20] S. Nadeem, I. Raishad, N. Muhammad, and M. T. Mustafa, "Mathematical analysis of ferromagnetic fluid embedded in a porous medium," *Results in Physics*, vol. 7, pp. 2361–2368, 2017.

[21] T. N. Sindhu and A. Atangana, "Reliability analysis incorporating exponentiated inverse Weibull distribution and inverse power law," *Quality and Reliability Engineering International*, vol. 37, no. 6, pp. 2399–2422, 2021.

[22] M. Y. Nadeem Abbas, S. N. Malik, and I. M. Alarifi, "On extended version of Yamada–Ota and Xue models of hybrid nanofluid on moving needle," *The European Physical Journal Plus*, vol. 135, no. 2, p. 145, 2020.

[23] R. L. Bailey, "Lesser known applications of ferrofluids," *Journal of Magnetism and Magnetic Materials*, vol. 39, no. 1-2, pp. 178–182, 1983.

[24] A. Shafiq, T. N. Sindhu, and Q. M. Al-Mdallal, "A sensitivity study on carbon nanotubes significance in Darcy-Forchheimer flow towards a rotating disk by response surface methodology," *Scientific Reports*, vol. 11, no. 1, pp. 1–26, 2021.

[25] M. Gnaneswara, "Unsteady radiative-convective boundary-layer flow of a Casson fluid with variable thermal conductivity," *Journal of Engineering Physics and Thermophysics*, vol. 88, no. 1, pp. 240–251, 2015.

[26] T. Hayat, A. Shafiq, and A. Alsaedi, "MHD axisymmetric flow of third grade fluid by a stretching cylinder," *Alexandria Engineering Journal*, vol. 54, no. 2, pp. 205–212, 2015.

[27] A. Rahman, T. N. Sindhu, S. A. Lone, and M. Kamal, "Statistical inference for burr type x distribution using geometric process in accelerated life testing design for time censored data," *Pakistan Journal of Statistics and Operation Research*, vol. 16, no. 3, pp. 577–586, 2020.

[28] W. R. Williams, M. T. Stenzel, X. Song, and L. D. Schmidt, "Bifurcation behavior in homogeneous-heterogeneous combustion: I. Experimental results over platinum," *Combustion and Flame*, vol. 84, no. 3-4, pp. 277–291, 1991.

[29] A. Shafiq, T. N. Sindhu, and C. M. Khalique, "Numerical investigation and sensitivity analysis on bioconvective tangent hyperbolic nanofluid flow towards stretching surface by response surface methodology," *Alexandria Engineering Journal*, vol. 59, no. 6, pp. 4533–4548, 2020.

[30] X. Song, W. R. Williams, L. D. Schmidt, and R. Aris, "Bifurcation behavior in homogeneous-heterogeneous combustion: II. Computations for stagnation-point flow," *Combustion and Flame*, vol. 84, no. 3-4, pp. 292–311, 1991.

[31] M. Gnaneswara Reddy, P. Vijayakumari, M. V. V. N. L. Sudharani, and K. G. Kumar, "Quadratic convective heat transport of Casson nanoliquid over a contract cylinder: an unsteady case," *BioNanoScience*, vol. 10, no. 1, pp. 344–350, 2020.

[32] M. A. Chaudhary and J. H. Merkin, "A simple isothermal model for homogeneous-heterogeneous reactions in boundary-layer flow. I equal diffusivities," *Fluid Dynamics Research*, vol. 16, no. 6, pp. 311–333, 1995.

[33] W. A. Khan and I. M. Pop, "Effects of homogeneous–heterogeneous reactions on the viscoelastic fluid toward a stretching sheet," *Journal of Heat Transfer*, vol. 134, no. 6, 2012.

[34] J. H. Merkin, "A model for isothermal homogeneous-heterogeneous reactions in boundary-layer flow," *Mathematical and Computer Modelling*, vol. 24, no. 8, pp. 125–136, 1996.

[35] R. Cortell, "MHD flow and mass transfer of an electrically conducting fluid of second grade in a porous medium over a stretching sheet with chemically reactive species," *Chemical Engineering and Processing: Process Intensification*, vol. 46, no. 8, pp. 721–728, 2007.

[36] M. Y. Imad Khan, T. S. Malik, M. Khan, and K. U. Rehman, "Homogenous–heterogeneous reactions in MHD flow of Powell–Eyring fluid over a stretching sheet with Newtonian heating," *Neural Computing and Applications*, vol. 30, no. 11, pp. 3581–3588, 2018.

[37] M. Ramzan, A. Rafiq, J. D. Chung, S. Kadry, and Y.-M. Chu, "Nanofluid flow with autocatalytic chemical reaction over a curved surface with nonlinear thermal radiation and slip condition," *Scientific Reports*, vol. 10, no. 1, pp. 1–13, 2020.

[38] A. Chaves, M. Zahn, and C. Rinaldi, "Spin-up flow of ferrofluids: asymptotic theory and experimental measurements," *Physics of Fluids*, vol. 20, no. 5, article 053102, 2008.

[39] A. M. Siddiqui, T. Haroon, and M. Zeb, "Analysis of Eyring-Powell fluid in helical screw rheometer," *The Scientific World Journal*, vol. 2014, Article ID 143968, 14 pages, 2014.

[40] T. Hayat, M. Awais, and S. Asghar, "Radiative effects in a three-dimensional flow of MHD Eyring-Powell fluid," *Journal of the Egyptian Mathematical Society*, vol. 21, no. 3, pp. 379–384, 2013.

[41] I. Starlin, D. A. Yuen, and S. Y. Bergeron, "Thermal evolution of sedimentary basin formation with variable thermal conductivity," *Geophysical Research Letters*, vol. 27, no. 2, pp. 265–268, 2000.

[42] W. Hafiz, H. Zeb, S. Bhatti, M. Gulistan, S. Kadry, and Y. Nam, "Numerical study for the effects of temperature dependent viscosity flow of non-Newtonian fluid with double stratification," *Applied Sciences*, vol. 10, no. 2, p. 708, 2020.

[43] N. Kousar, T. A. Nofal, W. Tahir, S. M. Bilal, and N. Sene, "Impact of ferromagnetic nanoparticles submerged in chemically reactive viscoelastic fluid transport influenced by double magnetic dipole," *Journal of Nanomaterials*, vol. 2022, Article ID 2558419, 12 pages, 2022.

[44] E. Sharifah, S. Alhazmi, W. Bilal, T. N. Althobaiti, N. Kousar, and A. Riaz, "Effects of homogeneous-heterogeneous reactions on Maxwell ferrofluid in the presence of magnetic dipole along a stretching surface: a numerical approach," *Nanofluids and Entropy Analysis with Electroosmotic Phenomenon*, vol. 2022, article 4148401, 13 pages, 2022.

[45] S. Rosseland, *Astrophysik and Atom-Theorestischegrundlagen*, Springer, Berlin, 1993.

[46] A. Zeeshan, A. Majeed, and R. Ellahi, "Effect of magnetic dipole on viscous ferro-fluid past a stretching surface with thermal radiation," *Journal of Molecular Liquids*, vol. 215, pp. 549–554, 2016.

[47] S. Esfandiari and S. Ramin, *Numerical Methods for Engineers and Scientists Using MATLAB*, CRC Press, 2013, http://gen.lib.rus.ec/book/index.php?md5=3604371A795EED86BDF0700CBC211758.

[48] T. Javed, N. Ali, Z. Abbas, and M. Sajid, "Flow of an Eyring-Powell non-Newtonian fluid over a stretching sheet," *Chemical Engineering Communications*, vol. 200, no. 3, pp. 327–336, 2013.

[49] M. Waqas, T. Shagufta Jabeen, S. A. S. Hayat, and A. Alsaedi, "Numerical simulation for nonlinear radiated Eyring-Powell nanofluid considering magnetic dipole and activation energy," *International Communications in Heat and Mass Transfer*, vol. 112, article 104401, 2020.

[50] C.-H. Chen, "Laminar mixed convection adjacent to vertical, continuously stretching sheets," *Heat and Mass Transfer*, vol. 33, no. 5-6, pp. 471–476, 1998.

[51] A. Ishak, R. Nazar, and I. Pop, "Hydromagnetic flow and heat transfer adjacent to a stretching vertical sheet," *Heat and Mass Transfer*, vol. 44, no. 8, pp. 921–927, 2008.